

## The Limits of Simulating Gas Giant Entry at True Gas Composition and True Flight Velocities in an Expansion Tube

C. M. James<sup>1</sup>, D. E. Gildfind<sup>1</sup>, R. G. Morgan<sup>1</sup>, and T. E. McIntyre<sup>2</sup>

<sup>1</sup>Centre for Hypersonics, School of Mechanical and Mining Engineering  
The University of Queensland, Brisbane 4072, Australia

<sup>2</sup>School of Mathematics and Physics  
The University of Queensland, Brisbane 4072, Australia

### Abstract

Due to high entry velocities when entering gas giant planets in the solar system (20–50 km/s), simulating gas giant entry in ground testing facilities is a complex problem. This paper details an investigation to simulate radiating Uranus entry flow conditions in a superorbital expansion tube facility. Theoretical calculations show that the X2 expansion tube at the University of Queensland can simulate Uranus entry at 20 km/s. This paper provides the justification for an experimental campaign that has been partially completed, but is still being analysed.

### Introduction

The Galileo probe's 47.5 km/s entry into Jupiter on December 7th, 1995 was an engineering triumph. The probe survived its entry into the largest gas giant planet in our solar system, and the full scientific mission that it was built for. However, analysis of the actual ablation of the Galileo probe's heat shield performed by Milos [7] showed that the ablation on both the stagnation point and the frustum of the probe's sphere-cone heat shield did not agree well with what had been predicted, and that only half of the heat shield actually ablated during the entry. This means that the heat shield, that made up half the mass of the whole probe [7], was larger than was required.

The Galileo probe's heat shield was designed using two separate CFD codes [18], and three different types of experiments to validate the simulations and some parameters used in them. Laser irradiation experiments [4] and arc-jet experiments in a 50%H<sub>2</sub>/50%He mixture were performed to test the heat shield materials and find their heat of ablation. Experiments were also performed in a ballistic range [13] using air to study convective heat transfer, and argon to study radiative heat transfer as it had been found that argon closely approximated the radiative heat transfer of 89%H<sub>2</sub>/11%He Jupiter entry mixtures [11]. The ballistic range experiments were able to recreate the levels of radiative heat transfer that they expected for the actual flight.

Computational Fluid Dynamics (CFD) studies have aimed to properly recreate the ablation of the Galileo probe's heat shield. These include a paper by Matsuyama et al in 2005 [5] that was able to recreate the frustum ablation by using the injection induced turbulence model proposed by Park, the correct atmospheric composition at the entry point, and more complex coupled radiative energy transfer. Stagnation point recession was still overestimated. A paper by Park in 2009 [12] was able to recreate the stagnation point recession "fairly closely" by improving on past methods and including radiation absorption in the vacuum ultraviolet region and the effect of spallation.

While the majority of gas giant entry research carried out in the last fifty years was either done to design the Galileo probe, or to analyse issues with it, the US National Research Council "*Vision and Voyages for Planetary Science in the Decade 2013-*

*2022*" report identified probes to Uranus [2] and Saturn [16, 15] as high priorities for future space missions giving new context to the study of gas giant entry in the coming years. While simulations have made up the majority of gas giant entry research in the two decades since the Galileo probe's entry, it is worth considering how experiments can aid the development of the next generation of gas giant entry probes.

The expansion tube, a modified shock tube that uses an extra low pressure shock tube to accelerate the shocked test gas to superorbital planetary entry conditions (through an unsteady expansion), typically between 6–15 km/s, is potentially well suited for simulating entry for planned missions to Uranus and Saturn. Expansion tube experiments using the true gas composition will also allow the flow phenomena experienced during an actual gas giant entry to be studied, something that was not able to be done when the Galileo probe was designed, which involved experiments more focused on engineering design as opposed to how the fundamental physics affected the entry.

Due to the fact that simulating the lower end of gas giant entry at the true flight velocity (20 km/s) in an expansion tube is pushing the limits of what these facilities can do in their current configurations, a thorough understanding of how the facility functions is required so the maximum performance can be extracted from the conditions that are tested, and that is what this paper examines. In this paper a parametric study of the X2 expansion tube as it can currently be configured is carried out using an equilibrium analysis code developed by the authors to create a performance map of the facility, and this is then used to extract the proposed test conditions that maximise the performance of the facility. Initial experiments have been carried out with positive results seen, but the analysis is ongoing and due to space constraints are not included in this paper.

The theoretical results shown in this paper indicate that it is possible to simulate 20 – 22 km/s Uranus entry in the X2 expansion tube at the University of Queensland with the current tunnel configuration. This compares well with the 22.3 km/s Uranus entry trajectory analysed by Palmer et al [10] this year based on an entry discussed in the aforementioned "*Vision and Voyages for Planetary Science in the Decade 2013-2022*" report.

### The X2 Expansion Tube

Since 1960, shock tubes and reflected shock tunnels have been used for the study of hypervelocity flows [17]. However, traditionally they are limited to velocities up to, and including, Earth orbit velocities ( $\approx 8$  km/s) [8]. Due to the fact that in these facilities all the energy is added to the flow across a shock wave, both reflected and non-reflected shock tunnels are limited by the total enthalpy that they can simulate [8]. This is because at very high shock speeds, the test flow exists as a highly dissociated plasma, which is useful to study high temperature effects, but not useful for aerodynamic testing.

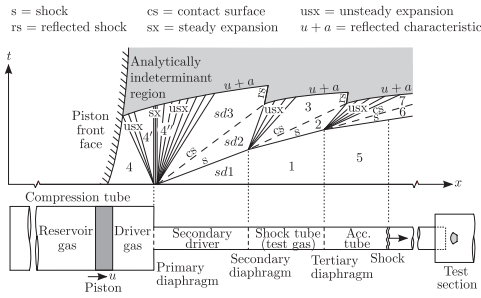


Figure 1: Distance-time ( $x-t$ ) diagram of the X2 expansion tube operating with a shock heated secondary driver tube in use. (Adapted from Gildfind et al [1].)

The expansion tube, a concept proposed by Resler and Boxson in the 1950's [14], circumvents the limitation mentioned above by only adding part of the required energy to the flow with a shock wave. The rest of the energy is added by processing the test gas with an unsteady expansion. At the expense of test time, total enthalpy and total pressure are added to the flow without the flow dissociation that would occur in a shock tunnel [8].

The X2 expansion tube at the University of Queensland has been used extensively to simulate and measure radiating planetary entry flows into several planetary bodies in the solar system, including Earth, Mars, Titan, and Venus, at velocities ranging from 6.5 – 12 km/s. However, considering simulating flows into the gas giant planets in the outer reaches of the solar system, velocities range from 20 – 50 km/s, pushing the limits of the performance envelope of these facilities as they are currently configured. It is important to examine the trends of the facility's performance in order to find the conditions that give maximum performance.

A schematic of the X2 expansion tube operating with a shock heated secondary driver is shown in Figure 1. The figure shows the longitudinal wave processes that occur in time. At the start of an experiment, each section of the tube downstream of the of the primary diaphragm is filled to a set pressure; upstream a set driver gas fill condition and reservoir fill condition are used to power the facility and drive shock waves of increasing strength through the driven sections of the tube and over a test model.

Different isentropic and compressible flow gas processes can be used to simulate different sections of the facility, and these processes combined with NASA's Chemical Equilibrium with Applications (CEA) [6] code for high-temperature gas effects have been used to simulate the facility for this paper. Generally the code simulates the driver, secondary driver, and shock tubes quite well, and it is only in the acceleration tube, where due to boundary layer effects and the low density nature of the tube, that experiment and theory can begin to differ significantly.

A parametric study of X2's performance has been conducted using PITOT [3], an in-house expansion tube and shock tunnel simulation code. A summary of how each section of the tube is simulated is detailed below. It should be noted that equilibrium gas effects are used for all calculations, and that the regions referred to in the list relate to different regions shown in Figure 1.

It should be noted that some analysis in this paper is prevented by the limitations of the CEA code. From the authors' experience, it will not solve conditions behind shock waves above 19.1 km/s, a velocity which the authors of this paper hope to surpass in experiment. It is hoped that in the future modifications to PITOT will allow faster conditions to be simulated.

1. The primary diaphragm burst pressure and temperature (region 4) are based on tuned empirical estimates of the burst conditions of the primary diaphragm and are hard

coded into the program as a stagnated driver condition ( $M \approx 0$ ). Due to the area change of the tube at the primary diaphragm, region 4 undergoes an isentropic expansion to a choked throat condition (and sometimes then a second steady expansion to a supersonic Mach number to simulate an orifice plate) at region 4'' and is then unsteadily expanded into the next tube downstream. Driver conditions used for this study can be seen in Table 1.

2. The secondary driver (if used) and shock tube conditions and shock speeds are found by noting the fact that as a shock moves through a tube, the pressure and velocity of the gas behind the shock wave ( $p_2$  and  $V_2$ ) and match the pressure and velocity of the gas unsteadily expanding into the tube behind it ( $p_3$  and  $V_3$ ). A secant solver is used to find the shock speed that makes the pressure and velocity equal on either side of the interface.
3. The acceleration tube conditions are found using the same process as the shock tube conditions above. However, to take into account low density shock tube effects in the acceleration tube that generally cause the shock tube gas (region 2) to be overexpanded in the acceleration tube at region 7, the shock tube gas is generally artificially expanded to the shock speed in the acceleration tube (denoted  $V_{s,2}$ ) instead of to the theoretical gas velocity of the shocked accelerator gas ( $V_7$ ). All calculations done in this paper assume that this has occurred.
4. If a supersonic nozzle is used at the end of the acceleration tube a steady, isentropic expansion through a known area ratio is used to get from the nozzle inlet conditions to the nozzle exit conditions. The nozzle geometric area ratio of 5.64 has been used for all calculations in this paper.
5. If required, the code has functionality to allow it to calculate conditions behind a normal shock in the test section for both frozen and equilibrium flow, and to find conditions over a 15 degree conehead pressure probe using a Taylor-Maccoll cone flow solver.

Driver case ID	Diaphragm thickness	Rupture pressure	Rupture temp.	Reservoir fill pressure	Driver fill pressure
-	mm	MPa	K	MPa	kPa
X2-LWP-2.0 mm-0	2.0	27.9	2700	6.85	928
X2-LWP-2.5 mm-0	2.5	35.7	3077	6.08	772

Table 1: X2 expansion tube driver conditions used for this study[1]. It should be noted that primary driver burst conditions come from calculations performed using an 80%He/20%Ar (by volume) driver gas, whereas the test conditions for this study have been performed using a 100%He driver condition with an orifice plate placed at the area change at the primary diaphragm.

### Expansion Tube Condition Analysis

All conditions mentioned in this analysis use a simulated Uranus entry test gas composition of 85% $H_2$ /15%He (by volume) based on values from the NASA planetary fact sheet [9] where the composition is listed as 82.5% $H_2$ /15.2%He/2.3% $CH_4$  (by volume). The methane percentage has been replaced with hydrogen to simplify the analysis. This is a simplification also used in the literature [10].

It should be noted that due to the fact that stagnation enthalpy ( $H_t$ ) is a measure of energy contained in a gas due to both its gas state and velocity (see the two terms in Equation 1), stagnation enthalpy is used to compare the performance of all test conditions in this paper. Where entry velocities are discussed, they

were calculated using just the velocity component of the stagnation enthalpy equation due to the very low freestream temperature in real planetary entry conditions (as opposed to expansion tube conditions where the freestream temperature can be 1000 – 2000 K and may be partially dissociated).

$$H_t = h + \frac{U_\infty^2}{2} \quad (1)$$

Figure 2 shows how different shock tube fill pressures affect the performance of the facility for two conditions without a secondary driver. One condition uses X2-LWP-2.0 mm-0 (the red lines) and the other uses X2-LWP-2.5 mm-0 (the black lines), and both have a constant acceleration tube fill pressure of 0.5 Pa. The plot shows a series of different variables normalised by their maximum value. These variables are the stagnation enthalpy of the flow ( $H_t$ ), the shock and acceleration tube shock speeds ( $V_{s1}$  and  $V_{s2}$ ), and the shocked test gas pressure and velocity ( $p_2$  and  $V_2$ ). Overall, the plot shows why a parametric study is important: the condition that maximises stagnation enthalpy is not the fastest condition (as may be expected), and the fastest condition does not occur when the shock tube fill pressure is minimised to maximise shock speed in the shock tube (which may also be expected).

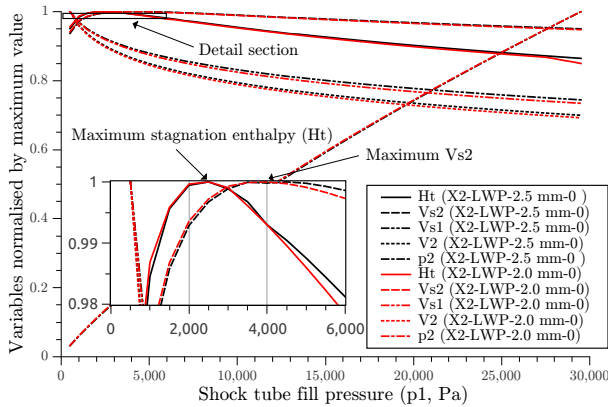


Figure 2: How the shock tube fill pressure affects two conditions without a secondary driver. All variables are normalised by their maximum values.

The reason why maximising velocity does not necessarily maximise the stagnation enthalpy is because the stagnation enthalpy is a function of both velocity and gas state (i.e. temperature), and if a gas is expanded to the maximum velocity, it has also potentially lost more temperature, meaning the increase in velocity may be cancelled out by the loss of energy from temperature.

Similarly, an unsteady expansion begins at a starting velocity and pressure, and expands a gas isentropically to a higher velocity and lower pressure. If the fill pressure in the shock tube ( $p_1$ ) is dropped too far to maximise the shock speed in the shock tube ( $V_{s1}$ ), there will be a point where the pressure behind the shock ( $p_2$ ) will be too low and will negatively affect the performance of the gas when it expands into the acceleration tube.

Both of these situations can be seen in Figure 2. For both conditions, the acceleration tube shock speed ( $V_{s2}$ ) is maximised at a shock tube fill pressure ( $p_1$ ) of 4 kPa, whereas, the maximum stagnation enthalpy occurs when the shock tube fill pressure is 2.5 kPa and the acceleration tube shock speed is slightly lower. It can also be seen that while the maximum shock tube shock speed and velocity ( $V_{s1}$  and  $V_2$ ) occur when the shock tube fill pressure is 0.5 kPa, this does not correspond to the fill pressure where either the stagnation enthalpy of the flow or the acceleration tube shock speed are maximised.

Figure 3 shows the performance of various conditions using a pure helium secondary driver tube. Similar to Figure 2, the driver condition has been fixed (as X2-LWP-2.0 mm-0) and the acceleration tube fill pressure has been fixed at 3 Pa, the lowest fill pressure at which all of the CEA based calculations would solve. Each curve represents a different shock tube fill pressure from 0.5 – 6 kPa, and the secondary driver fill pressure has been evaluated from 1 – 200 kPa.

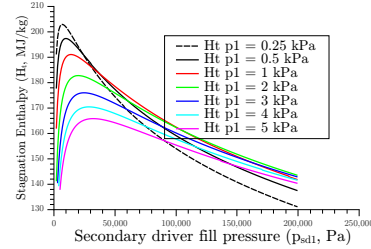


Figure 3: How secondary driver fill pressure ( $p_{sd1}$ ) affects performance for different shock tube fill pressures ( $p_1$ ). Each condition uses the same driver condition (X2-LWP-2.0 mm-0) and a set acceleration tube fill pressure ( $p_5$ ) of 3 Pa.

Two things can be seen from Figure 3: Firstly, as expected, the maximum secondary driver performance shifts to the right as the shock tube fill pressure increases, meaning that a higher secondary driver fill pressure ( $p_{sd1}$ ) is required to maximise performance with a higher shock tube fill pressure ( $p_1$ ). Secondly, it can be seen that the maximum stagnation enthalpy seems to be asymptoting to a shock tube fill pressure of 0. This is because when a lower secondary driver fill pressure is required to maximise secondary driver performance, the secondary driver shock  $V_{sd}$  is faster, meaning that the temperature (and sound speed) of the shocked secondary driver gas (state sd2) is higher, increasing its performance. However, other limitations come into play here. A test cannot be performed at zero pressure in the shock tube, therefore a minimum shock tube fill pressure has to be established. With very low fill pressures, test conditions become more susceptible to leaks in the shock tube (which are already an issue when such a light test gas is used<sup>1</sup>) and there is a point where the condition will not have sufficient test gas to produce a usable test flow. For this reason, 2 kPa was chosen as the shock tube fill condition for secondary driver conditions, as it seemed to offer the best compromise between maximising performance, and achieving a usable test flow.

Because a 2 kPa shock tube fill pressure was chosen for the secondary driver conditions, and that in Figure 2 it could be seen that a 2.5 kPa shock tube fill pressure gave maximum performance for conditions without a secondary driver (with 2 and 3 kPa just behind it) it was decided to use a 2 kPa shock tube fill pressure for the conditions without a secondary driver as well to simplify analysis.

Now that a 2 kPa shock tube fill pressure ( $p_1$ ) has been selected for all conditions, Figure 4 compares the performance of the two conditions with a secondary driver. It should be noted that this time the two acceleration tube fill pressures ( $p_5$ ) are different, based on the limitations of the simulation code for each condition. The black curve (using the driver condition X2-LWP-2.5 mm-0) has an acceleration tube fill pressure of 4 Pa, whereas the red curve (using the driver condition X2-LWP-2.0 mm-0) has an acceleration tube fill pressure of 2 Pa.

In Figure 4 it can be seen that for both conditions performance

<sup>1</sup>The molecular weight of the 85% $H_2$ /15% $He$  test gas mixture (2.31 g/mol) is 8% of the molecular weight of air (28.97 g/mol), so small amounts of air contamination can significantly change the gas constant of the mixture.

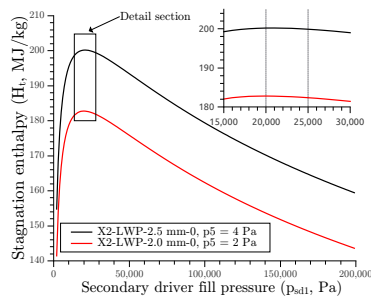


Figure 4: How secondary driver fill pressure ( $p_{sd1}$ ) affects performance for a set 2 kPa shock tube fill pressure ( $p_1$ ) with two different driver conditions.

is maximised when the secondary driver fill pressure ( $p_{sd1}$ ) is in the range 15 – 25 kPa, with a maximum between 20–21 kPa for both conditions. For this reason, a secondary driver fill pressure of 21 kPa was selected for use with the driver condition X2-LWP-2.5 mm-0, and a secondary driver fill pressure of 25 kPa was selected for use with X2-LWP-2.0 mm-0.

Now that the four conditions have been finalised, Figure 5 shows the performance of the four different proposed scenarios. It should be noted that three of the conditions are truncated at a maximum point due to the performance limits of the CEA program used to do the equilibrium gas calculations.

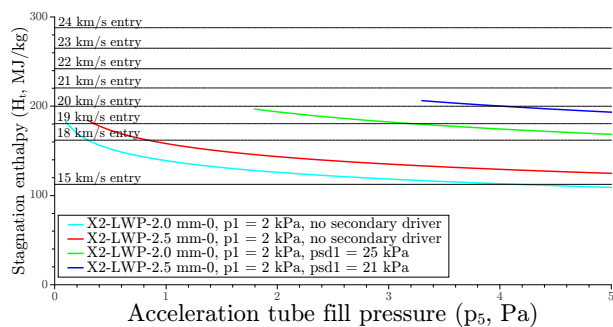


Figure 5: This figure shows the performance of the four different expansion tube conditions chosen when the acceleration tube fill pressure ( $p_5$ ) is varied between 0.1 – 5 Pa. These performance curves are compared to the stagnation enthalpy of various planetary entries from 15 – 24 km/s.

In Figure 5 it can be seen that the chosen acceleration tube fill pressure ( $p_5$ ) has a drastic effect on the stagnation enthalpy of the test flow. Looking at the no secondary driver condition using the driver condition X2-LWP-2.0 mm-0, the stagnation enthalpy of the test flow varies from 110 – 182 MJ/kg over the 5 Pa range shown in the figure (and a similar jump from 125 – 184 MJ/kg is shown for the condition using X2-LWP-2.5 mm-0). The performance potential of the two secondary driver conditions can also be seen. Even with the lowest acceleration tube fill pressures that would solve for each condition (1.8 Pa for X2-LWP-2.0 mm-0, 3.2 Pa for X2-LWP-2.5 mm-0) both conditions are able to simulate a 20 km/s Uranus entry. It is hoped that with lower fill pressures (0.5 – 1.0 Pa) they could simulate a 22 km/s entry. Experiments have been performed to confirm this, and preliminary results look promising, but the data is still being analysed.

## References

[1] Gildfind, D., Morgan, R., McGilvray, M., Jacobs, P., Stalker, R. and Eichmann, T., Free-piston driver optimisation for simulation of high mach number scramjet flow conditions, *Shock Waves*, **21**, 2011, 559–572.

[2] Hubbard, W., Ice giants decadal study, in *Vision and Voyages for Planetary Science in the Decade 2013 – 2022*, National Academy Press, Washington, D.C., 2010, 1–40.

[3] James, C., Gildfind, D., Morgan, R., Jacobs, P. and Zander, F., Designing and simulating high enthalpy expansion tube conditions, in *2013 Asia-Pacific International Symposium on Aerospace Technology*, Takamatsu, Japan, 2013.

[4] Lundell, J., Spallation of the galileo probe heat shield, in *AIAA Paper 82-0852*, 1982.

[5] Matsuyama, S., Ohnishi, N., Sasoh, A. and Sawada, K., Numerical simulation of galileo probe entry flowfield with radiation and ablation, *Journal of Thermophysics and Heat Transfer*, **19**, 2005, 28–35.

[6] McBride, D. and Gordon, G., *Computer Program for Calculations of Complex Chemical Equilibrium Compositions and Applications II. Users Manual and Program Description*, Nasa Lewis Research Center, Cleveland, OH, U.S.A., 1996.

[7] Milos, F., Galileo probe heat shield ablation experiment, *Journal of Spacecraft and Rockets*, **34**, 1997, 705–713.

[8] Morgan, R., A review of the use of expansion tubes for creating superorbital flows, in *AIAA 35th Aerospace Sciences Meeting and Exhibit*, Reno, NV, Jan 6-10, 1997.

[9] NASA, Uranus fact sheet, <http://nssdc.gsfc.nasa.gov/planetary/factsheet/uranusfact.html>, 2014, accessed Aug 7, 2014.

[10] Palmer, G., Prabhu, D. and Cruden, B., Aeroheating uncertainties in uranus and saturn entries by the monte carlo method, *Journal of Spacecraft and Rockets*, **51**, 2014, 801–814.

[11] Park, C., Calculation of radiation from argon shock layers, *Journal of Quantitative Spectroscopy and Radiative Transfer*, **28**, 1982, 29–40.

[12] Park, C., Stagnation-region heating environment of the galileo probe, *Journal of Thermophysics and Heat Transfer*, **23**, 2009, 417–424.

[13] Park, C. and Balakrishnan, A., Ablation of galileo probe heat-shield models in a ballistic range, *AIAA Journal*, **23**, 1985, 301–308.

[14] Resler, E. and Boxsom, D., *Very high mach number principles by unsteady flow principle*, Cornell University Graduate School of Aerodynamic Engineering, 1952.

[15] Spilker, T. R., Saturn atmospheric entry probe mission study, in *Vision and Voyages for Planetary Science in the Decade 2013 – 2022*, National Academy Press, Washington, D.C., 2010, 1–19.

[16] Spilker, T. R., Saturn atmospheric entry probe trade study, in *Vision and Voyages for Planetary Science in the Decade 2013 – 2022*, National Academy Press, Washington, D.C., 2010, 1–13.

[17] Stalker, R., Isentropic compression of shock tube driver gas, *ARS Journal*, **30**, 1960, 564.

[18] Talley, R., *Galileo Probe Deceleration Module Final Report*, Re-Entry Systems Operations, General Electric Co., Rept. 84SDS2020, 1984.